Tellus (1997), 49A, 423–438
Printed in UK – all rights reserved

TELLUS
ISSN 0280–6495

Multiple equilibria in radiative-convective atmospheres

By NILTON O. RENNÓ[1], *Department of Atmospheric Sciences, The University of Arizona, P. O. Box 210081, Tucson, AZ 85721-0081, USA*

(Manuscript received 24 May 1996; in final form 12 February 1997)

ABSTRACT

A one-dimensional, radiative-convective model is used to study the equilibria conditions of moist atmospheres. We show that when the hydrologic cycle is included in the model a subcritical bifurcation occurs, leading to 2 linearly stable solutions to the radiative-convective equilibria. In this case, when the net forcing is larger than a critical value, two equilibria are possible. Furthermore, a finite amplitude instability can lead to a runaway greenhouse regime when the solar forcing is larger than a second critical value. In general, previous climate studies with radiative-convective models did not include a hydrologic cycle. Instead, the atmosphere's water vapor mixing ratio was diagnosed based on the climatological profile of relative humidity. We show that fixing the water vapor relative humidity profile at the climatological value (in the computation of the radiation fluxes only) leads to a unique stable solution to the radiative-convective equilibria. Thus, the crucial part of the hydrologic cycle which allows multiple solutions is the relaxation of the assumption of a climatological relative humidity profile. Our results do not apply directly to any real planet because of large uncertainties in our calculation due to the absence of clouds and the use of a one-dimensional model. The 1st equilibrium corresponds to an optically thin atmosphere. In this regime, the system is nearly linear and is in a state of small dissipation. The 2nd equilibrium corresponds to an optically thick atmosphere. In this 2nd regime, the system is highly nonlinear and is in a state of large dissipation.

1. Introduction

In nature, complex and poorly understood climate feedback mechanisms exist, making climate modeling a complex and difficult endeavor. Here, we study one of these mechanisms, the effect of the water vapor feedback on one-dimensional radiative-convective equilibria. Our results do not apply directly to any real planet because of large uncertainties in our calculation due to the absence of clouds and the use of a one-dimensional model. Since clouds have a large influence on radiative transfer, they are potentially a key factor in determining the character of the radiative-convective equilibria of any real planet. We make experiments with no cloud cover to avoid the inclusion of a large number of arbitrary parameters that would make both the numerical experiments and their interpretation very difficult. This is a logical step to take before the effect of clouds is studied. Instead of parameterizing the radiative properties of clouds, we perform experiments for a wide range of values of the input solar radiation. This is a classical approach which neglects many of the effects of clouds on climate equilibrium and the effects of cloud feedbacks on climate change (Manabe and Strickler, 1964; Manabe and Wetherald, 1967; Lindzen et al., 1982). However, this approach implicitly takes into account the first order effects of clouds on radiative transfer, that is, the effect of clouds on the net radiative flux at the model's surface.

One-dimensional, radiative-convective models are very useful for understanding the heat budget of planetary atmospheres. Their main value is that

E-mail: renno@soar.atmo.arizona.edu

they allow one to examine general principles and test fundamental ideas. Their major drawback is the inability to compute the feedbacks between the horizontal heat transports and the temperature structure from first principles. Radiative-convective models usually lack the ice albedo-temperature feedback, although this feedback was successfully included in a radiative-convective model by Wang and Stone (1980). In the present study, a radiative-convective equilibrium model which explicitly includes a hydrologic cycle (Rennó, 1992; Rennó et al., 1994a) is used to study the equilibria conditions of moist atmospheres. In this model, cumulus convection is parameterized by a variety of complex schemes, similar to those currently used in GCMs.

Convection tends to adjust atmospheres toward an adiabatic state. However, the nature of the mean state of the adjusted atmosphere is controversial (Betts, 1982; Emanuel et al., 1994; Rennó and Williams, 1995). Currently, in most radiative-convective models, it is assumed that moist convection adjusts unstable temperature lapse rates to moist adiabatic ones. In general, those models make crude assumptions about the vertical distribution of water vapor by the convective motions. Rennó et al. (1994a, 1994b) showed that the water vapor content of moist atmospheres depends crucially on the precipitation efficiency of cumulus convection, that is, on the processes that determine the precipitation fallout. The uncertainties in the water vapor distribution present a serious problem because atmospheric water vapor has a large influence on radiative transfer (Raval and Ramanathan, 1989; Ramanathan and Collins, 1991). Indeed, water vapor is the most important greenhouse gas present in the Earth's atmosphere.

The main drawback of the previous climate studies with radiative-convective models was that they did not include a hydrologic cycle; instead, the atmosphere's water vapor mixing ratio was diagnosed based on the climatological profile of relative humidity (Manabe and Strickler, 1964; Sarachik, 1978; Lindzen et al., 1982). The exceptions to this rule are the models of Ramanathan (1981) and Betts and Ridgway (1988). These two models represent a large step in the right direction. Their only limitation is due to the fact that the water vapor profile is empirically constrained. In the Ramanathan model, the water vapor relative humidity profile is based on an experimental equation validated for the Earth's present-day climate. In Betts and Ridgway's model, the water vapor vertical distribution is computed through a mixing line assumption (Betts, 1982, 1985); here too, the water vapor profile is constrained by the present climatology. Since water vapor has a large influence on radiative transfer, and its content and vertical distribution in the atmosphere is to a large extent controlled by moist convection, it is desirable to explicitly compute the atmospheric water vapor content. Another limitation of previous radiative-convective models is the use of very simple numerical procedures to parameterize cumulus convection which, in general, force the atmospheric temperature profile to be moist adiabatic. We show that a physically based model of cumulus convection leads to interesting results. Finite amplitude instabilities can lead to either multiple equilibria or an abrupt transition to a runaway greenhouse regime. These instabilities are caused by feedbacks between the water vapor opacity, radiative transfer, and the dynamics of moist convection.

Hilbert (1912) showed that, for an isolated system, the thermodynamic equilibrium is unique. It follows from Hilbert's proof that the radiative equilibrium solution to a plane-parallel atmosphere in local thermodynamic equilibrium is unique (Pelkowski, 1993). Currently, there is a general belief that, for a given heat input value, radiative-convective atmospheres also have only one possible equilibrium solution. However, since in this case the system is not isolated — there is an entropy flux through the system's boundary — Hilbert's proof does not hold. The current belief of a unique equilibrium solution for radiative-convective atmospheres is partially due to the fact that in previous studies with radiative-convective models the atmosphere's temperature profile was constrained to be moist adiabatic, and the water vapor mixing ratio was diagnosed based on the climatological profile of relative humidity. In this case, the atmospheric water vapor mixing ratio is a function of temperature alone, and the equilibrium is unique. We show that, when the hydrologic cycle is included in the radiative-convective equilibrium model, multiple equilibria can occur. Moreover, we show that a cumulus model in which the cloud mass flux is not a function of height inhibits, but does not eliminate, the multiple equilibria (Rennó, 1994).

Simpson (1927) suggested, and Komabayasi (1967) and Ingersoll (1969) showed in classical papers that, as long as there is a water supply, when the concentration of the absorbing gas in the atmosphere is temperature dependent, equilibrium is impossible for values of the net heat input larger than a critical value. This result is referred to as a runaway greenhouse effect. Nakajima et al. (1992) elegantly studied the limit of the infrared emission by saturated moist-adiabatic atmospheres. They found that the upper limit in the infrared emission is due to the fact that when the opacity of convecting atmospheres becomes sufficiently large, the temperature structure of the emitting layers (the region where the optical thickness to infrared radiation is $\tau \approx 1$) asymptotically approaches a fixed moist-adiabatic temperature profile. These previous studies looked at the runaway greenhouse regime as an asymptotic limit to the radiation flux that moist atmospheres can emit. They did not explore the dynamics of atmospheres approaching a runaway greenhouse state. In this study, we explore the dynamic behavior of convecting atmospheres as the solar forcing is varied. We show that when the net heat input (the solar forcing) is larger than other smaller critical values, a finite amplitude instability can lead to either multiple equilibria or a runaway greenhouse regime. We also show that the critical solar forcing values depend on the precipitation efficiency of cumulus convection. The multiple equilibria are due to a subcritical bifurcation that leads to two linearly stable radiative-convective equilibria.

The convective available potential energy (CAPE) is defined as the total amount of work done by the buoyancy forces in moving an air parcel along a convective updraft (see Brunt, 1941). Rennó and Ingersoll (1996) showed that CAPE is a fundamental global number qualifying the state of a planet's atmosphere in statistically steady conditions. We argue that of the two radiative-convective equilibria, one corresponds to the weakest heat engine while the other corresponds to the most powerful heat engine possible within the constraints of moist convection for a given forcing value. In the weakest heat engine regime, the atmosphere's opacity to infrared radiation is the smallest. The bulk of the emission of radiation to space originates in the warm surface and low troposphere. In the most powerful heat engine regime, the atmosphere's opacity to infrared radiation is the largest. The bulk of the emission of radiation to space originates in the cold upper troposphere. According to Carnot and Sandström's theorems the weakest heat engine is in a low-efficiency regime, and the mechanical dissipation is low. The bulk of the energy emitted to space originates from regions close to where the planet absorbs solar radiation (i.e., from the surface and low troposphere). In this regime, both the mechanical dissipation of energy and the convective available potential energy (CAPE) are low. The most powerful heat engine is in a higher efficiency regime, and therefore, dissipation is higher. The difference in pressure and temperature between the regions where solar radiation is absorbed and infrared radiation is emitted by the planet is larger. In this regime, both the mechanical dissipation of energy and CAPE are higher.

2. Description of the model

2.1. *Model equations*

We use a radiative-convective equilibrium model with an explicit hydrologic cycle (Rennó, 1992; Rennó et al., 1994a). The model's basic equations at each pressure level i are:

$$\left(\frac{\partial \theta}{\partial t}\right)_i = Q_i - R_i + F_{\theta i}, \tag{1}$$

and

$$\left(\frac{\partial r}{\partial t}\right)_i = C_i + F_{ri}. \tag{2}$$

Independent variables are time, t, and pressure, p. The prognostic variables are the potential temperature, θ, and the water vapor mixing ratio, r. Q_i in eq. (1) represents the heating rate by cumulus convection and large-scale condensation (it includes all phase changes of water substance represented in our model), and C_i in eq. (2) stands for the moistening rate due to cumulus transport and phase changes of water substance. These terms are computed by the cumulus convection scheme. R_i in Equation (1) represents the net radiative cooling rate. Radiation is computed by a sophisticated parameterization scheme (Chou, 1992; Chou et al., 1991), described in the next subsection. The vertical diffusion of temperature, $F_{\theta i}$, and moisture, F_{ri}, are parameterized by the Fickian law

$F_{\theta_i} = g(\partial\tau_\theta/\partial p)_i$, and $F_{ri} = g(\partial\tau_r/\partial p)_i$, where the variable τ_θ represents the vertical flux of potential temperature, and τ_r the vertical flux of water vapor. In the free atmosphere, they are estimated as $\tau_{\theta i} = \rho_i^2 g k_{v\theta}(\partial\theta/\partial p)_i$, and $\tau_{ri} = \rho_i^2 g k_{vr}(\partial r/\partial p)_i$, where $k_{v\theta}$ and k_{vr} are vertical diffusion coefficients for each variable, ρ_i is the air density at level i, and g is gravitational acceleration. We present results of experiments with values of diffusion coefficients equal to $k_{v\theta} = k_{vr} = k_v = 5\ \mathrm{m^2\ s^{-1}}$. This small diffusion is not supposed to represent any real physical process, but it is included for numerical convenience. The observed turbulent eddies are represented by the parameterized convection.

Surface fluxes are computed by the bulk aerodynamic formulae $\tau_{\theta s} = \rho_a C_D |v_a|(\theta_s - \theta_a)$, and $\tau_{rs} = \rho_a C_D |v_a|(r_s - r_a)$, where the subscript $_s$ refers to values at the surface, and the subscript $_a$ refers to values at a level just above the surface, the anemometer level. C_D is a drag coefficient, set equal to 0.0025, v_a is the wind speed at the anemometer level, $5\ \mathrm{ms^{-1}}$, θ_s is the surface potential temperature computed by the "swamp" formulation, r_s is the water vapor mixing ratio at the surface, which is the saturation mixing ratio of the surface. θ_a and r_a, the potential temperature and water vapor mixing ratio, respectively, at the anemometer level are computed based on the temperature and water vapor mixing ratio at the model's lowest level. The potential temperature and the water vapor mixing ratio are made constant from the model's lowest level down to the surface.

We use centered differences in the vertical direction. Time integration of the non-diffusive terms is performed by the Leapfrog scheme with an Asselin filter (Asselin, 1972) inserted at every time step to damp its computational mode. The smoothing constant of the Asselin filter is set at 0.1. The time integration of the diffusive terms is performed by the Euler forward scheme. The time step is set to 15 min, and radiative fluxes are computed each 12 h. Cumulus convection and large-scale condensation are computed every time step. Experiments are made with the number of vertical layers equal to 16 in the model's troposphere. The thickness of these vertical layers is constant in pressure. The troposphere's top is computed by the model. It is just above the level of neutral buoyancy for deep convection. It can be situated anywhere between the model's surface at 1000 mb and the 10 mb level. Above this level, there is an upper layer, extending from 10 to 1 mb, in radiative equilibrium. This upper layer is subdivided into 5 sub-layers for the computation of the radiative fluxes. Except where indicated, the model integrations were started from the mean sounding of GATE phase III.

Since the main role of the ocean in the radiative-convective equilibrium is to be wet (we are interested in the equilibrium solution), we use a "swamp" as the lower boundary. The "swamp" is a saturated surface in which the heat capacity is zero and the supply of moisture is infinite. Therefore, the net energy flux into the surface is required to be zero at each instant. This is not exactly true in our model since, for numerical stability, we set the "swamp" temperature equal to the averaged temperature computed in the preceding 96 time steps (24 h). The reader should be warned that the swamp surface might facilitate the transition from one equilibrium to the other.

2.2. *Radiation model*

We use a fast and accurate broadband radiation parameterization model developed by Chou (1992) and Chou et al. (1991). The reference carbon dioxide concentration (330 ppm), ozone mixing ratio, and stratospheric water vapor profile are from the AFGL standard atmosphere (McClatchey et al., 1972).

For longwave absorption broadband transmission functions for water vapor, carbon dioxide and ozone are used. The approach relies on parameterizations of diffuse transmittance functions appropriately weighted by Planck blackbody source terms. The schemes used include the water vapor line and continuum absorption; carbon dioxide absorption through band centers and band wing regions; and infrared ozone-absorption bands. The curve-fitting was done with a Planck function evaluated from 160 to 330 K. Therefore, the scheme works well for temperatures up to 330 K, but the errors tend to grow unpredictably above this temperature. However, except for the unstable branch corresponding to the runaway greenhouse regime, the results presented in this paper (e.g., the multiple solutions) occur within the temperature range in which the Planck function was evaluated (e.g., between 160 and 330 K). The unstable branch was already examined in detail in previous studies on the runaway green-

house regime. Therefore, Chou's radiation model should be adequate for use in our process model. Moreover, most of the previous studies on the runaway greenhouse regime used simple gray radiation models (e.g. Komabayasi, 1967; Ingersoll, 1969; Nakajima et al., 1992). Even above 330 K our radiation model represents an improvement over gray models.

In the present study we focus on experiments with a cloudless model. We decided to first make experiments with no cloud cover to avoid the inclusion of a large number of arbitrary parameters that would make both the numerical experiments and its interpretation very difficult. The use of a cloudless model allows a minimum of parameters to be used in the numerical calculations, and therefore the opportunity for greater physical insight than when clouds are included in the model. This is a logical step to take before the effect of clouds is studied. A study of the effect of clouds on the multiple equilibria is underway.

We perform experiments for a wide range of values of the input solar radiation. This approach neglects many of the effects of clouds on climate equilibrium, and the effects of cloud feedbacks on climate change. However, our approach implicitly takes into account the first order effects of clouds on radiative transfer. That is, the effect of clouds on the net radiative flux at the model's surface. Clouds might amplify or reduce the sensitivity of our model, depending on whether their feedback is positive or negative. Moreover, the distribution of stratiform clouds in nature is affected by the ambient relative humidity, which is controlled by cumulus convection.

2.3. *Cumulus convection schemes*

We focus on experiments with a physically based cumulus scheme developed by Emanuel (1991). However, the scheme used here differs from the scheme described in Emanuel (1991) and Rennó et al. (1994a). Here we use a modified version of the scheme in which convection can originate from any unstable level, and the fractional area covered by convective updrafts is computed based on a quasi-equilibrium assumption. We also modified the numerics of the scheme to avoid overflows at unrealistically high temperatures (for the present climate on Earth).

The main assumption in the scheme proposed by Emanuel is that the fundamental entities in cumulus convection are the sub-cloud-scale drafts rather than the cloud-scale circulations themselves. Convection occurs whenever the environment is unstable to a parcel in reversible adiabatic ascent from the surface. Vertical transports are accomplished by saturated updrafts and downdrafts, by a single unsaturated downdraft driven by evaporation of the falling precipitation, and by compensating subsidence. The main closure parameters are the precipitation efficiencies of each saturated updraft, the fraction of the precipitation that falls through unsaturated air, and the rate of evaporation of falling precipitation. Dry adiabatic adjustment is performed before and large-scale condensation after moist convection, whenever necessary. In the Emanuel scheme, the large-scale water vapor field is affected by advection of environmental water vapor by compensating updrafts and downdrafts, by detrainment of water substance from convective drafts, and by evaporation of precipitation (see Emanuel, 1991).

We also use a variety of complex cumulus convection schemes similar to those used in Global Climate Models (GCMs). The following cumulus convection parameterization schemes are used: the Moist (Hard) Convective Adjustment scheme (Kelvin, 1862; Manabe et al., 1965), hereafter referred to as the HARDADJ scheme; the GISS Model I scheme (Arakawa, 1969; Somerville et al., 1974), hereafter referred to as the GISSI scheme; and the GISS Model II scheme (Hansen et al., 1983), hereafter referred to as the GISSII scheme. Except for the HARDADJ scheme, all the cumulus convection schemes used in our model include the drying effect of the compensating subsidence mass flux forced by moist convection.

3. The multiple equilibria

In this section, we examine the equilibria conditions of moist atmospheres. The effects of clouds on the radiative fluxes are not included in the experiments discussed below.

3.1. *Experiments with the Emanuel scheme*

3.1.1. Sensitivity to initial conditions for various values of the solar forcing. In the experiments described in this subsection, we specify the initial conditions. First using the GATE Phase III mean

sounding as the initial condition, we integrate the model for 100 days with fixed surface temperature — this is long enough to achieve equilibrium with the specified surface temperature. Then we integrate the model up to day 8000. This is long enough for the model to reach statistical equilibrium, when this is possible. We use the Emanuel convection scheme with the "standard" set of microphysical parameters (see Rennó et al., 1994a).

Fig. 1 shows the time evolution of the surface temperature for various values of both the solar forcing and the initial condition. It is important to note that according to our notation, F_{so} is the specified incoming solar radiation flux, and F_{net} is the model computed net solar radiation flux. For the earth's present day climate the incoming solar radiation flux is ≈ 340 W/m^2, and the planet's albedo is about 0.3. In our model, the net flux of solar radiation at the atmosphere's top depends on F_{so}, the specified surface albedo ($a=0.102$), and the intensity of Rayleigh scattering.

Figure 1a shows that when the flux of incoming solar radiation is $F_{so}=310$ W m^{-2} only one equilibrium solution is possible. In this case, the equilibrium atmosphere is optically thin (not shown). Fig. 1b shows that two equilibria are possible when the flux of incoming solar radiation is $F_{so}=320$ W m^{-2}. Increases in the solar forcing lead to increases in the difference of temperatures between the two equilibria (not shown). Fig. 1c shows that for $F_{so}=340$ W m^{-2} again the equilibrium is unique. However, now the equilibrium atmosphere

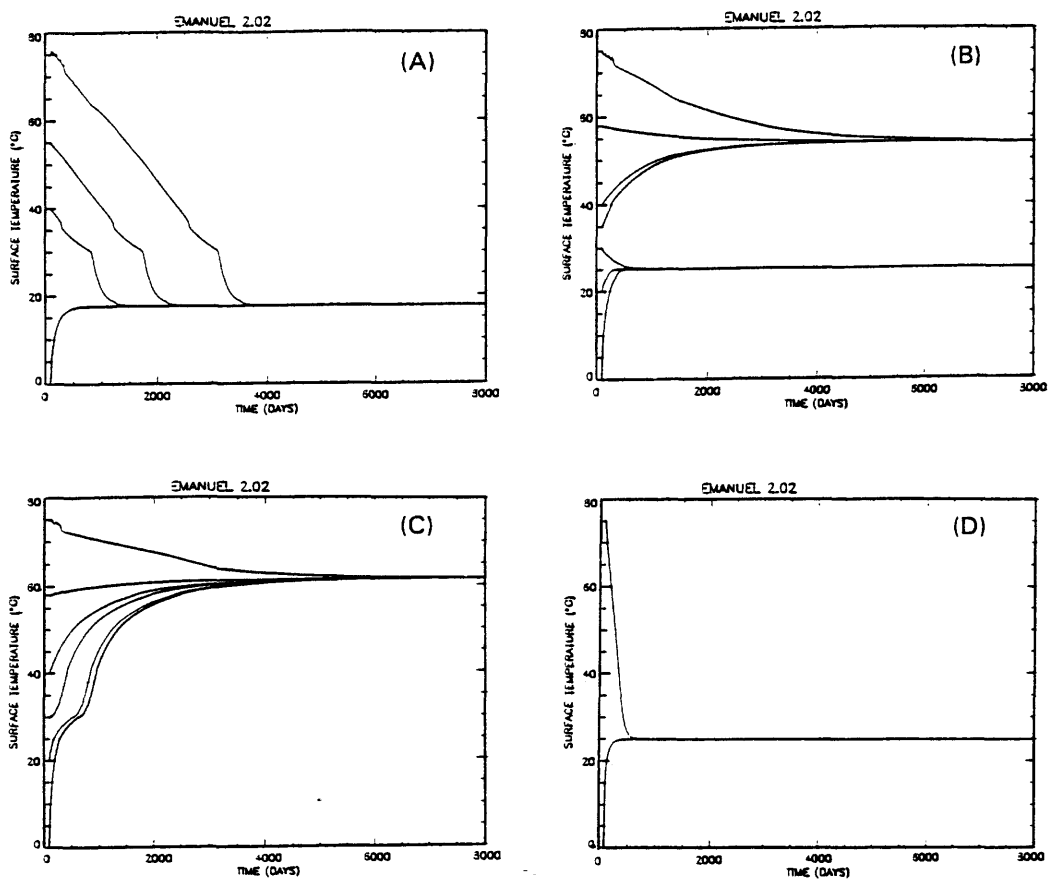

Fig. 1. Results of experiments with the Emanuel scheme. Evolution with time of the surface (swamp) temperature for various initial conditions for the incoming solar flux equal to (a) 310 W m^{-2}, (b) 320 W m^{-2}, (c) 340 W m^{-2}, and (d) for an experiment in which the water vapor mixing ratio is fixed in the calculation of the radiation fluxes. In this last case the incoming solar flux is equal to 330 W m^{-2}.

is optically thick (not shown). The above experiments give an idea of the robustness of the multiple solutions. Each solution can be approached by a wide range of initial conditions. Thus, both solutions are robust.

Finally, Fig. 1d shows that when the water vapor mixing ratio profile is fixed at the cold equilibrium value, during the calculation of the radiative fluxes, the multiple equilibria are eliminated ($F_{so}=330$ W m^{-2} in this experiment). Thus fixing the water vapor mixing ratio in experiments with the Emanuel scheme leads to a unique stable solution to the radiative-convective equilibrium. We must conclude that the multiple equilibria are not caused by the coupling of moist convection with the surface fluxes. We also did not find multiple equilibria when the relative humidity profile was fixed at the climatological value. Thus, the crucial part of the hydrologic cycle which allows the multiple solutions is the relaxation of the assumption of a climatological water vapor profile.

3.1.2. Instability to finite amplitude perturbations. In the experiments described in this subsection, we study climate sensitivity to finite amplitude perturbations in the water vapor content of the upper troposphere. We show that the model's climate is stable to a short and unstable to a long perturbation in the atmospheric water vapor content. The motivation for these experiments is to find out if a change in the climate equilibria can be induced by natural processes which might inject large quantities of water vapor, but not many aerosols, into the atmosphere (e.g., the impact of a large asteroid in a ocean, and perhaps large-scale undersea volcanism). First we set the solar forcing to a supercritical value for the multiple equilibria to occur. Then using the GATE phase III mean sounding as the initial condition, we integrate the model for 100 days with the surface temperature fixed at 0°C. We also integrate the model up to day 1550, which is long enough for an equilibrium to be reached. At day 1550, we abruptly make the atmosphere saturated from 600 mb up to 10 mb, during the computation of the radiation fluxes (i.e., the model sees the change in the water vapor content only through changes in the radiation fluxes). We keep this water vapor perturbation for 300 days. Next we relax it back to the model's computed values and continue the time integration up to day 3550, when we abruptly make the atmosphere saturated from 600 mb up to 10 mb, yet keep the perturbation for 1000 days. Finally we integrate the model up to day 8000. This is long enough for the model to reach a new equilibrium or to come back to the previous equilibrium whenever possible.

The evolution of the swamp temperature as a function of time is shown in Fig. 2a. Starting from the cold initial condition, a radiative-convective equilibrium in which the swamp temperature is $\sim$22°C is reached. After the smaller finite amplitude perturbation between days 1550 and 1850, the model returns to the cold equilibrium. However, after the larger finite amplitude perturbation between days 3550 and 4550, the model drifts to a warmer equilibrium in which the swamp temperature is $\sim$42°C. Figs. 2b–d show the time evolution of the precipitation and evaporation fields, the net solar and net infrared radiation fluxes both at the surface and at the top of the atmosphere. Note that the net flux of solar radiation, at the top of the model's atmosphere, is balanced by the emission-to-space of longwave radiation (Fig. 2d). The net loss of surface infrared flux is larger in the colder climate equilibrium. This happens because in the colder equilibrium the atmosphere's opacity is smaller, thus more energy is radiated to space by the planet's surface. In this case, the net atmospheric radiative cooling rate is smaller. Since in radiative-convective equilibrium the latent heat released by condensation (precipitation) loosely balances the net atmospheric radiative cooling, the precipitation rate is also smaller.

The thermodynamic characteristics of both equilibria are shown in Fig. 3. The colder equilibrium (solid line) presents a smaller value of the convective available potential energy (CAPE) than the warmer equilibrium (dashed line). The pseudo-adiabatic CAPE value is $\sim$1000 J kg^{-1} for the colder equilibrium and $\sim$9000 J kg^{-1} for the warmer equilibrium. Furthermore, the colder equilibrium presents a relatively dry atmosphere while the warmer equilibrium presents a saturated atmosphere (Fig. 3d). This happens because, as shown in Fig. 3e, the warmer equilibrium presents an opaque atmosphere. Since at equilibrium the warming by the compensating subsidence balances the radiative cooling, and the radiative cooling at the interior of the opaque atmosphere approaches

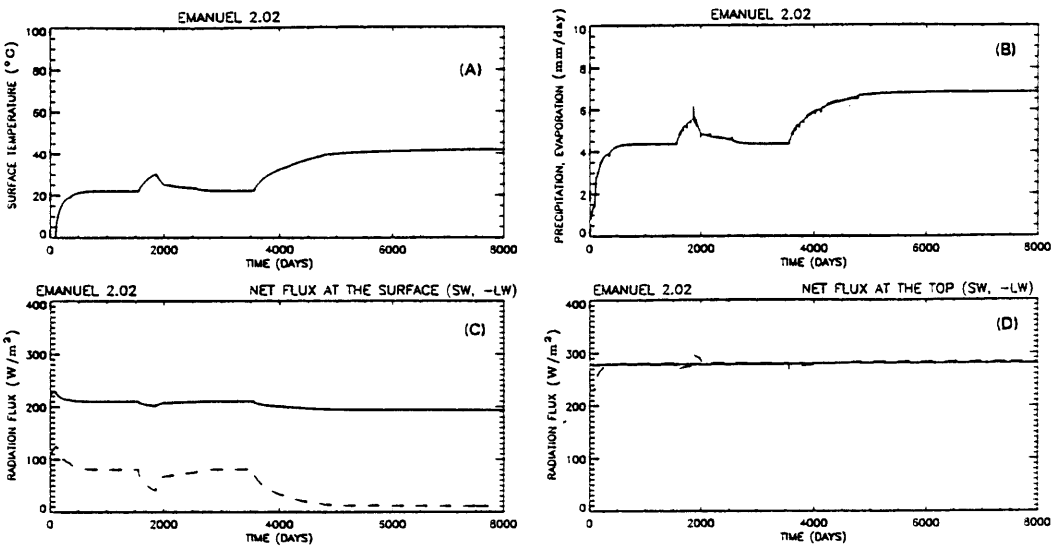

Fig. 2. Results of experiments with the Emanuel scheme. Evolution with time of (a) surface (swamp) temperature, (b) precipitation (solid line), evaporation (dashed line), (c) net solar (solid line), net infrared radiation flux (dashed line) at the surface, and (d) top of the atmosphere.

zero, the compensating subsidence also approaches zero. Then the "drying" effect of the compensating subsidence approaches zero, and the equilibrium atmosphere becomes saturated. Thus, in an optically thick atmosphere, both the convective updrafts and the convective downdrafts must be saturated.

At the cold equilibrium, the surface temperature is $T_h \approx 295$ K, and the emission temperature (that is, the mean temperature of the atmospheric layers radiating to space) is approximately $T_c \approx 270$ K (estimated from Fig. 3e). This implies a thermodynamic efficiency of $\eta \approx 0.08$ for the convective heat engine (Rennó and Ingersoll, 1996). Since the heat input to the convective heat engine is approximately equal to the surface latent heat flux, we have $F_{in} \approx 130$ W m^{-2}. Thus, the energy available for the "cold" convective heat engine to transform into mechanical energy is $F_{av} = \eta F_{in} \approx 11$ W m^{-2}. For the "warm" climate equilibrium we have: $T_h \approx 315$ K; $T_c \approx 270$ K; $\eta \approx 0.14$; $F_{in} \approx 195$ W m^{-2}; and, $F_{av} \approx 28$ W m^{-2}. Since statistical equilibrium is achieved only when the energy available from the convective heat engine is used to balance mechanical dissipation, the warm climate is in a state of higher dissipation than the colder climate. This is the reason for the larger CAPE values in the warmer climate.

3.1.3. Sensitivity to model parameters. The sensitivity of our radiative-convective equilibria model to the various arbitrary parameters is presented in Table 1. All experiments (model runs) were performed with the Emanuel convection scheme and with the solar forcing value equal to 330 W m^{-2}. In experiment ESTD the standard set of model parameters is used. In this case, the equilibria surface temperatures are 25.6°C and 56.0°C. In experiments EVRES and ETRES, the vertical and time resolution are doubled, and in experiment EDRAG, the drag coefficient is doubled. The climate equilibria are only weakly affected by these parameters; the equilibria surface temperature changes by less than 4°C. These results suggest that the multiple equilibria are not sensitive to the boundary layer parameterization scheme.

In experiments EDIF1, EDIF2, EDIF3, and EDIF4, the role of the vertical diffusion of temperature and moisture is tested. Setting the diffusion coefficient to zero (the most realistic value) does not eliminate the multiple equilibria. Increases in the value of the diffusion coefficient leads to increases in the atmospheric water vapor content, and therefore in the equilibria surface temperature (due to a stronger greenhouse effect). However, it does not eliminate the multiple equilibria.

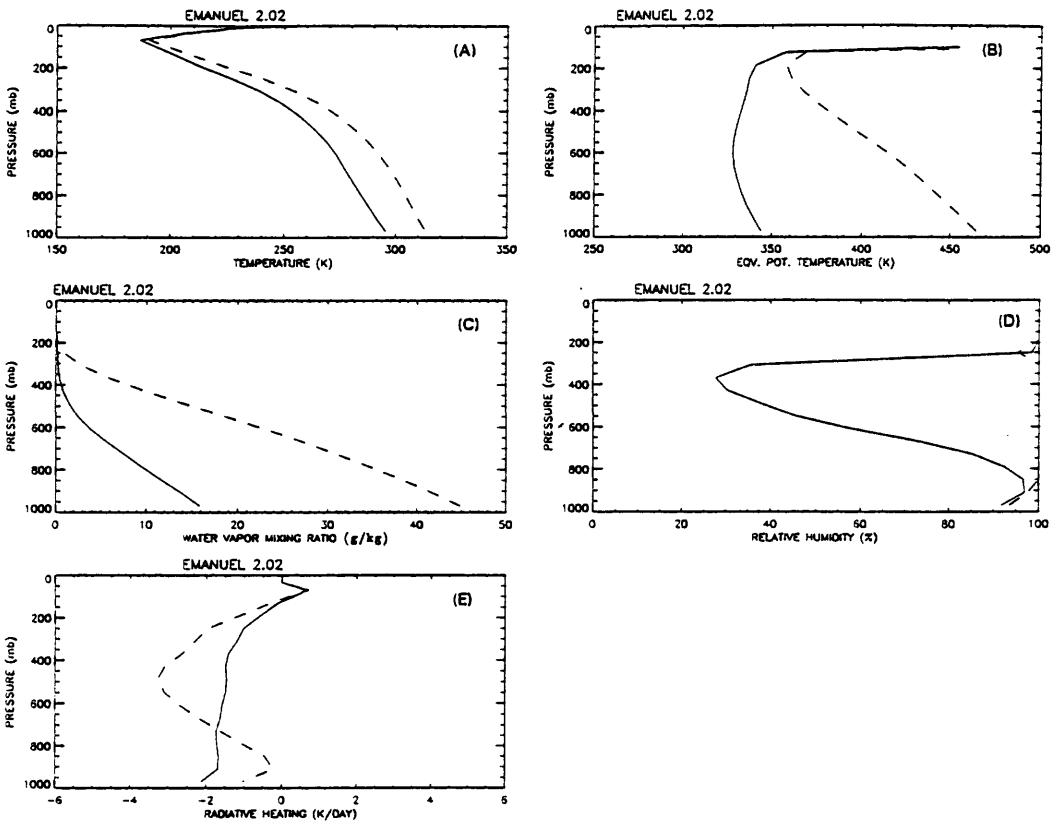

Fig. 3. Results of experiments with the Emanuel scheme. Thermodynamic characteristics of both, the cold (solid line) and the warm (dashed line) equilibria. Vertical profile of (a) temperature, (b) equivalent potential temperature, (c) water vapor mixing ratio, (d) relative humidity, and (e) total radiative cooling.

Table 1. *Equilibria surface temperatures obtained in experiments with the Emanuel convection scheme with solar forcing set to 330 W m^{-2} as a function of various parameters*

Run	NL (levels)	k_v (m^2 s^{-1})	$C_D\|v_a\|$ (ms^{-1})	Δt (s)	T_1 (°C)	Evp_1 (mm day^{-1})	T_2 (°C)	Evp_2 (mm day^{-1})
ESTD	16	5.0	0.0125	900	25.6	5.0	56.0	7.3
EVRES	32	—	—	—	26.6	4.7	52.3	7.1
ETRES	—	—	—	450	25.6	5.0	55.9	7.4
EDRAG	—	—	0.0250	—	24.4	5.6	53.7	7.5
EDIF1	—	0.0	—	—	19.2	3.9	50.5	6.6
EDIF2	—	2.5	—	—	22.4	4.4	51.7	6.8
EDIF3	—	7.5	—	—	27.1	5.3	59.0	7.7
EDIF4	—	10.0	—	—	29.2	5.8	62.1	8.0

The model solutions are not very sensitive to the model's arbitrary parameters. Indeed, the multiple equilibria do not critically depend on the value of the various parameters. Therefore, the multiple equilibria are a robust result. However, the multiple equilibria are very sensitive to the moistening parameters of the cumulus convection model. The sensitivity of the bifurcation diagram

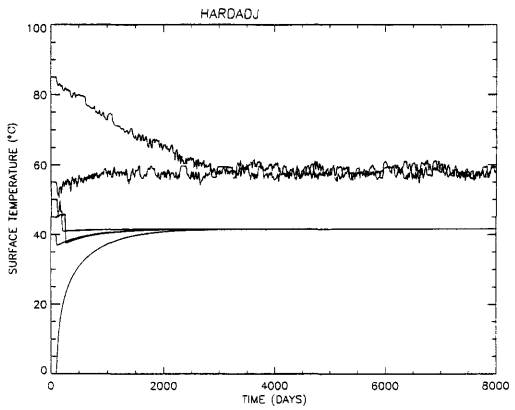

Fig. 4. Results of experiments with the HARDADJ scheme. Evolution with time of the surface (swamp) temperature for various initial conditions for the incoming solar flux equal to 325 W m^{-2}.

on the precipitation efficiency of cumulus convection is studied in subsection 3.3.

3.2. *Experiments with current GCM schemes*

In this section, we look for the multiple equilibria in radiative-convective experiments with some of the cumulus convection schemes most widely used in GCMs. Our objective is to find out how robust the multiple equilibria are.

Fig. 4 shows that multiple equilibria can occur in experiments with the classical HARDADJ scheme (Manabe et al., 1965). However, they occur because the HARDADJ scheme breaks down when the atmosphere becomes opaque. This happens because, when the atmospheric opacity approaches one, the saturation requirement for convective adjustment to occur is only rarely satisfied at the lower layers. Then, the temperature in those layers increases abruptly and greatly departs from the moist adiabatic (Rennó et al., 1994b). Fig. 5 shows that while at the cold equilibrium the atmosphere is moist adiabatic and saturated, at the warm equilibrium it is convectively unstable and unsaturated at the lower levels. However, when either the saturation requirement is relaxed or the diffusion coefficient is large enough to keep the atmosphere saturated (not shown), the multiple equilibria do not occur in experiments with the HARDADJ scheme. Therefore when the atmosphere's temperature profile is constrained to be moist adiabatic and the water vapor mixing ratio is a function of temperature alone, the radiative-convective equilibrium is unique. This explains the current belief in a

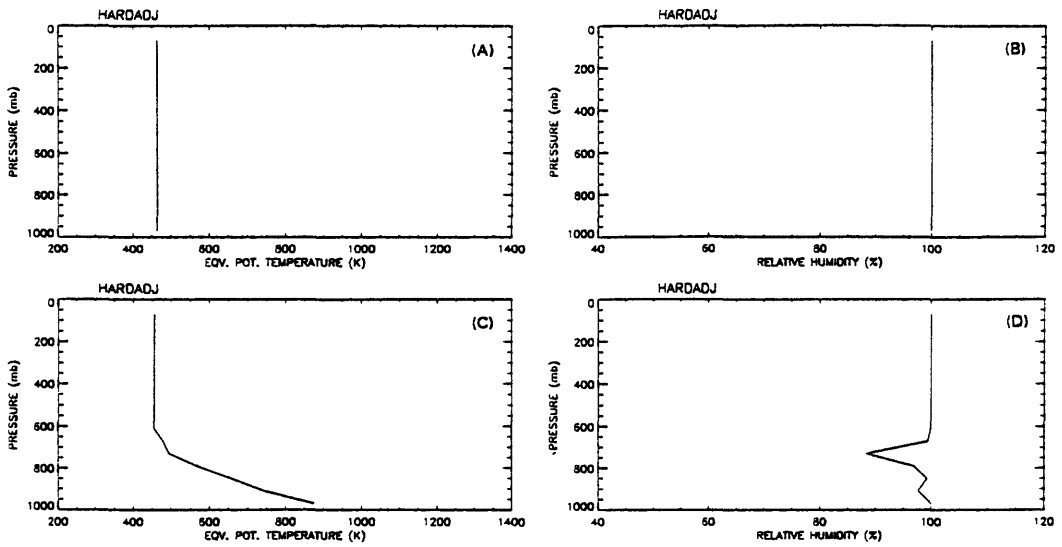

Fig. 5. Results of experiments with the HARDADJ scheme in which the diffusion coefficient is set to 2 m^2 s^{-1}. Thermodynamic characteristics of both, the cold and the warm equilibria. Vertical profile of (a) equivalent potential temperature for the cold equilibrium, (b) relative humidity for the cold equilibrium, vertical profile of (c) equivalent potential temperature for the warm equilibrium, and (d) relative humidity for the warm equilibrium.

unique equilibrium solution for radiative-convective atmospheres.

The multiple equilibria produced by the GISSI (Arakawa, 1969) convection scheme are similar to the multiple equilibria produced by the Emanuel convection scheme (not shown). The multiple equilibria also occur in experiments with the GISSII convection scheme (not shown). However, since in the GISSII scheme the convective mass flux is assumed to be constant with height in the warm equilibrium (opaque atmosphere), the atmosphere is unsaturated (not shown). It is important to note, however, that the constant mass flux inhibits the multiple equilibria. That is, the multiple equilibria occur for larger values of the solar forcing (we found that, in this case, $F_{net}=F_1\approx 290$ W m^{-2}). This happens because increases in the atmosphere's opacity lead to increases in the intensity of convection, which in turn, lead to increases in the intensity of the compensating subsidence throughout the atmosphere. Increases in the intensity of the compensating subsidence, in turn, lead to increases in the advective drying of the atmosphere which reduces the atmosphere's opacity.

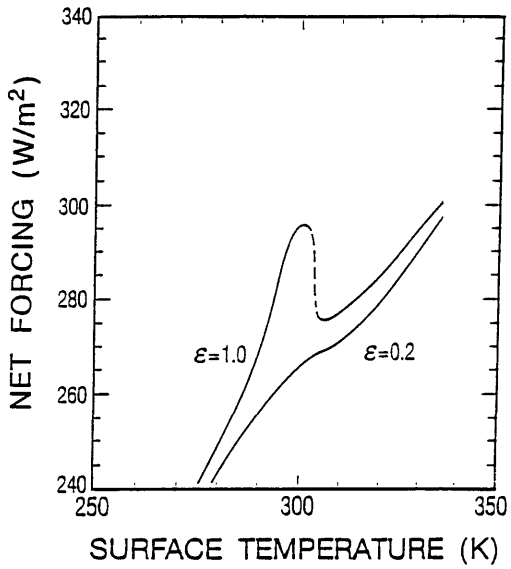

Fig. 6. Bifurcation diagram obtained with the Emanuel scheme when the precipitation efficiency is $\varepsilon_p=0.2$, and $\varepsilon_p=1.0$. The branch represented by a dashed line is linearly unstable.

3.3. *Bifurcation diagrams*

We obtained the bifurcation diagrams by performing a series of experiments similar to the ones described in Subsection 3.1.1. Fig. 6 shows bifurcation diagrams obtained in experiments with the Emanuel convection scheme in which the precipitation efficiency parameter, ε_p, was set to constant values throughout the convective layer. Note that the bifurcation is subcritical. Fig. 6 shows that the possibility of multiple equilibria depends crucially on the precipitation efficiency of moist convection. The differences between the two equilibria are also sensitive to the precipitation efficiency of convection.

Fig. 7 shows a sketch of the complete bifurcation diagram for the Emanuel convection scheme with the "standard" set of microphysical parameters (see Rennó et al., 1994a). The complete bifurcation diagram shows that the equilibria conditions of radiative-convective atmospheres can be expressed in terms of 4 critical net solar forcing values (F_{net}), F_1, F_2, F_3 and F_4. For the Emanuel convection scheme with the "standard" set of microphysical parameters, we have $F_1\approx 275$ W m^{-2}, $F_3\approx 295$ W m^{-2}, and $F_4\approx 310$ W m^{-2}. Nakajima et al. (1992) found that the asymptotic limit for the emission of infrared radiation by a convecting planet in which the only atmospheric constituent is water vapor is $F_2=F_{B,max}\approx 290$ W m^{-2} (Fig. 8).

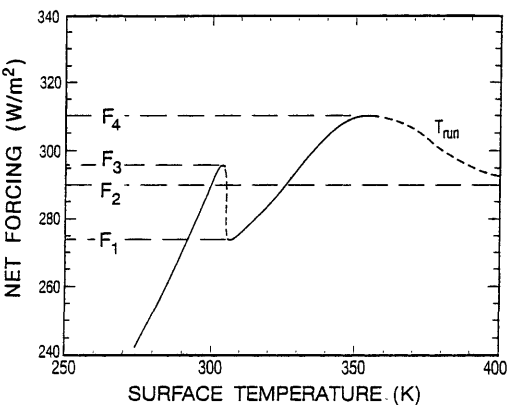

Fig. 7. Sketch of the complete bifurcation diagram obtained with the Emanuel scheme with the standard set of microphysical parameters and Nakajima's results. The branches represented by a dashed line are linearly unstable.

For values of the forcing smaller than F_1, the

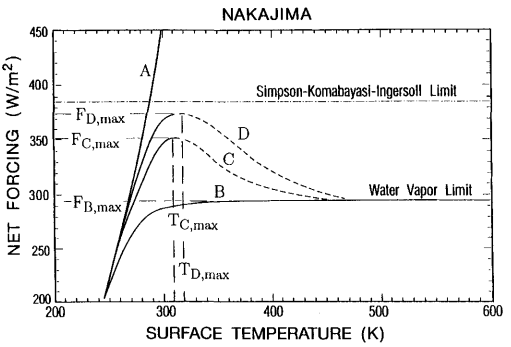

Fig. 8. Relationships between the outgoing infrared radiation flux at the top of the atmosphere, F_{out}, and the imposed surface temperature, T_s, for a planet in which the only infrared absorber present in the atmosphere is water vapor. The atmosphere is constrained to be moist adiabatic and saturated. The branches represented by a dashed line are linearly unstable (adapted from Nakajima et al., 1992).

equilibrium is unique and corresponds to the optically thin regime. For values of the forcing between F_1 and F_2, two linearly stable equilibria are possible. For values of the forcing between F_2 and F_3, two linearly stable equilibria and a runaway greenhouse regime are possible. For values of the forcing between F_3 and F_4, only one linearly stable equilibrium, the optically thick regime, and a runaway greenhouse regime are possible. Finally for values of the forcing above F_4, equilibrium is impossible before the complete evaporation of the planet's reservoir of infrared absorber (Komabayasi, 1967; and Ingersoll, 1969).

The multiple equilibria and the runaway greenhouse regime are also sensitive to the parameterizations of cumulus convection and cloud cover (not shown). In this study, we focused on experiments with no cloud cover. Interactive clouds might amplify or reduce the sensitivity of our model, depending on whether their feedback is positive or negative.

4. Discussion

4.1. A physical interpretation

Nakajima et al. (1992) carried out an elegant and detailed study of the limit of the emission of infrared radiation by planets with saturated moist adiabatic atmospheres. Their radiative-convective equilibrium model is very simple. The model atmosphere is assumed to be transparent to solar radiation. The dry air is assumed to be transparent to infrared radiation, and the water vapor absorption coefficient of infrared radiation is assumed to be gray. The Eddington approximation is used to integrate the radiative transfer equation. The stratosphere is assumed to be in radiative equilibrium. Finally, the troposphere is assumed to have a moist pseudoadiabatic temperature lapse-rate and to be saturated with respect to water substance. Nakajima et al. (1992) studied the relationships between the outgoing infrared radiation flux at the top of the atmosphere, F_{out}, and the surface temperature, T_s, for specified values of the surface temperature. In this study, we examine the dynamic behavior of convecting atmospheres as we vary the solar forcing. Here we show that the study by Nakajima et al. (1992) provides a beautiful physical interpretation for our results.

Fig. 8, adapted from Nakajima et al., shows the relationships between the net forcing (the outgoing infrared radiation flux at the top of the atmosphere), F_{out}, and the imposed surface temperature, T_s, for a planet in which the only infrared absorber present in the atmosphere is water vapor. It is important to note that, at equilibrium, the net heat input must be balanced by the outgoing infrared radiation flux, that is $F_{net}=F_{out}$. Curve A represents the relationship between F_{out} and T_s for a planet without atmosphere (or alternatively, for a planet without infrared absorber present in the atmosphere). In this case $F_{out}=\sigma_R T_s^4$, where σ_R is the Stefan-Boltzmann constant. Thus increases in the surface temperature produce a monotonic increase in the emission of infrared radiation by the planet's surface, as well as an unique equilibrium solution. Curve B shows the relationship between F_{out} and T_s for a case in which the only atmospheric constituent is the infrared absorber (water vapor). In this case, increases in the surface temperature lead to an asymptotic value for F_{out}. Equilibrium is not possible when the net heat input to the planet's atmosphere is larger than the asymptotic limit for the flux of outgoing infrared radiation (i.e., when $F_{net}>F_{B,max}$). Finally, curves C and D display the relationships between F_{out} and T_s when both the infrared absorber (water vapor) and the components that are transparent to infrared radiation are present in the planet's atmosphere. In curve C, the partial pressure of the

infrared absorber is larger than in curve D. Therefore, while the optically thin branch discussed in Subsection 3.3 corresponds to curve C, the optically thick branch corresponds to curve D.

In both cases, increases in the surface temperature produce increases in the emission of infrared radiation by the planet up to a temperature, T_{max}, at which the emission of infrared radiation reaches a maximum value, F_{max}. For temperatures above T_{max}, increases in the surface temperature produce decreases in the emission of infrared radiation. This happens because above T_{max} the reduction in the emission of infrared radiation by the warm surface and lower troposphere, due to increases in the atmosphere's optical thickness, overcompensates for the increases in the emission of infrared radiation produced by increases in the surface and atmospheric temperatures. Further increases in the surface temperature lead to the asymptotic value for the emission of infrared radiation, $F_{B,max}$, observed when only water vapor is present in the planet's atmosphere.

The asymptotic value for the emission of infrared radiation, $F_{B,max}$, is approached because the partial pressure of the infrared absorber (water vapor) increases rapidly with temperature. Thus as the atmosphere's temperature increases, the molar fraction of the infrared absorber asymptotically approaches one. In this limit, the planet behaves as if only the infrared absorber were present in its atmosphere. Fig. 8 also shows that increases in the molar fraction of the infrared absorber atmospheric component lead to decreases in the value of the maximum emission of infrared radiation, F_{max} (that is, $F_{C,max} < F_{D,max}$). This happens because, for a given value of the surface temperature, increases in the molar fraction of the infrared absorber lead to increases in the atmosphere's optical thickness, due to decreases in the atmosphere's temperature lapse-rate (Nakajima et al., 1992).

Nakajima et al. (1992) noted that, for values of F_{out} between $F_{B,max}$ and F_{max}, two solutions for the radiative-convective equilibria are possible. However, they did not discuss the stability of these solutions. From the consideration of the stability of linear perturbations, it is straightforward that the warmest solution is unstable (increases in the surface temperature lead to decreases in F_{out}). Thus, one of the two solutions found by Nakajima et al. is linearly stable while the other is linearly unstable. While the linearly stable solution corresponds to the classical solution to the radiative-convective equilibria, the unstable solution corresponds to the runaway greenhouse regime. We showed that the linearly stable solution is unstable to finite amplitude perturbations, leading to either multiple equilibria or a runaway greenhouse regime. In order to produce a runaway greenhouse regime, the finite amplitude perturbation must be large enough to produce a surface temperature larger than a critical value, T_{run}, which corresponds to the Nakajima et al. unstable solution (Fig. 6). In other words, T_{run} is the surface temperature necessary to "activate" the runaway greenhouse regime. It is important to note that, since the warm equilibrium is already saturated, just an increase in the atmosphere's relative humidity is not enough to activate the runaway greenhouse. The runaway greenhouse regime can be activated only by a substantially larger increase in the atmosphere's molar fraction of water vapor.

The radiative-convective equilibrium is unstable to finite amplitude perturbations, leading to multiple equilibria, because of a positive feedback generated by the interaction of the infrared radiation flux with detrained water vapor near the convective updraft's level of neutral buoyancy. The increase in the water vapor content at the detrainment layers produces an increase in the radiative cooling around the level of neutral buoyancy and a decrease in the radiative cooling at the lower layers, a greenhouse effect. The greenhouse effect produces an increase in the surface temperature, and therefore, in the atmosphere's moisture content, which in turn, leads to an increase in the convective moisture flux. The increase in the convective moisture flux leads to an increase in the detrainment of water vapor around the level of neutral buoyancy. This increase feeds back on the process, causing a rapid evolution in the moisture content of the detrainment layers. When this feedback sets in, the atmosphere's temperature and moisture content increase steadily. The temperature might reach a value at which the planet's atmosphere becomes warm and opaque enough so that the outgoing infrared radiation flux, F_{out}, balances the net heat input, F_{net}. In this case, another equilibrium occurs. When the net heat input, F_{net}, is larger than the asymptotic limit for a runaway greenhouse regime, $F_{B,max}$ (Fig. 8), and the finite ampli-

tude perturbation is large enough to produce a surface temperature larger than T_{run}, a runaway greenhouse regime occurs. In this case, the finite amplitude instability is due to the reduction in the emission of infrared radiation with increases in surface temperature by the opaque planet. In the runaway greenhouse regime, the radiation flux emitted by the opaque planet is smaller than the net heat input. Thus, in this case, equilibrium is not possible before the complete evaporation of the planet's reservoir of infrared absorber (Komabayasi, 1967; and Ingersoll, 1969).

4.2. Why 2 equilibria? A tentative explanation

Hilbert (1912) proved that, for an isolated system, thermodynamic equilibrium is unique. Prigogine (1947) proved that when steady states occur sufficiently close to thermodynamic equilibrium states, in the linear regime, they are characterized by an extremum principle according to which the rate of entropy production (dissipation) has its minimum value compatible with the system's constraints. Here equilibrium states refer to states of thermodynamic equilibrium at the interior of the fluid, given the temperature at the boundaries. The theorem of minimum entropy production is a very general principle of linear non-equilibrium thermodynamics of irreversible processes. Therefore, in linear systems the equilibrium state is unique. However, the theorem of minimum entropy production breaks down when equilibrium states occur far from the state of thermodynamic equilibrium — in the nonlinear regime. There are evidences that nonlinear systems move towards equilibrium regimes of maximum entropy production (dissipation) (Paltridge, 1981; Hunt and Hunt, 1987). Thus the nonlinear regime may be characterized by an extremum principle according to which the rate of entropy production has its maximum value compatible with the system's constraints. This result is referred to as the principle of maximum entropy production. Thus when nonlinear regimes are possible, multiple equilibria states might occur (Glansdorff and Prigogine, 1971).

Mobbs (1982) used variational principles and a zonally symmetric model to show that a principle of either minimum or maximum entropy production is obeyed by the model, depending on the heat flux parameterization. These results support the use of entropy production principles in the interpretation of the multiple equilibria.

The current belief of unique radiative-convective equilibrium is partially due to the fact that, in previous studies with radiative-convective models, the atmosphere's temperature profile was constrained to be moist adiabatic, and the water vapor mixing ratio was diagnosed based on the climatological profile of relative humidity. In this case, the system is nearly linear (for Earth-like values of the solar forcing), and the radiative-convective equilibrium is unique, corresponding to a state of minimum dissipation. When the hydrologic cycle is included in the radiative-convective equilibrium model, feedbacks between the water vapor opacity, the radiative transfer, and the dynamics of moist convection lead to the possibility of highly nonlinear regimes. In this case, finite amplitude instabilities can either lead to multiple equilibria or to an abrupt transition to a runaway greenhouse regime.

We found two robust (linearly stable) solutions for the radiative-convective equilibria. The first equilibrium corresponds to an optically thin atmosphere. In this regime, the system is nearly linear and is in a state of minimum dissipation. We argue that this equilibrium corresponds to the weakest natural heat engine possible within the constraints of moist convection for a given solar forcing value. Solar radiation is mainly absorbed at the warm surface, while the bulk of the emission of radiation to space originates in the warm surface and low troposphere (the entropy flux is minimum). This regime is stable to finite amplitude perturbations when the radiation emitted by an opaque version of the planet is larger than the absorbed solar radiation. The second equilibrium corresponds to an optically thick atmosphere. In this second regime, the system is highly nonlinear and is in a state of maximum dissipation. It corresponds to the most powerful natural heat engine possible within the constraints of moist convection for a given solar forcing value. In this regime, the atmosphere's opacity to infrared radiation is the largest. The bulk of the emission of radiation to space originates in the cold upper troposphere (the entropy flux is maximum).

5. Conclusions

Pollack (1971) determined that the critical forcing in order for a runaway greenhouse regime to

occur, in a pure water vapor atmosphere with 50% cloud cover, is between 1.4 and 2.0× the present terrestrial value, depending on the assumed relative humidity profile. Kasting et al. (1984) studied the response of a cloudless, saturated atmosphere with a moist adiabatic temperature lapse rate to large changes in the forcing. When the water vapor continuum absorption outside of the 8–12 μm window region was neglected, they predicted a monotonic increase in the surface equilibrium temperature from −1 to 111°C as the solar flux increased from 0.81 to 1.45× the present value for the Earth. In this case, a runaway greenhouse regime did not occur. However, when Kasting et al. (1984) crudely included the water vapor continuum absorption outside of the 8–12 μm window region, the critical forcing for a runaway greenhouse regime to occur was about 1.16× the present value for the Earth. The continuum absorption may lead to large increases in the atmosphere's opacity with increases in its water vapor content. Therefore, it is important to include the continuum absorption in studies of the runaway greenhouse regime, even if it is only crudely parameterized. The radiation parameterization scheme used in our model includes the water vapor continuum absorption outside of the 8–12 μm window region (Chou et al., 1991). Rennó et al. (1994b) showed that the critical forcing for a runaway greenhouse regime to occur in a moist planet is very sensitive both to the parameterization of cumulus convection as well as to the cloud microphysical processes.

In this study, we show that in a convecting moist planet when the heat input to the planet's atmosphere is above critical values (smaller than the classical critical forcing value for a runaway greenhouse regime to occur) either multiple equilibria or a runaway greenhouse regime can occur. A large source of uncertainty in our calculation is the absence of clouds. Since clouds have a large influence on radiative fluxes, they are potentially a key factor in determining whether either multiple equilibria or a runaway greenhouse regime will ever occur in a real atmosphere.

Acknowledgements

My special thanks go to Prof. Peter H. Stone for suggesting the study of the various convection schemes in a radiative-convective model. I would like to thank him also for his encouragement in the early stages of the present study. I would like to thank Prof. Kerry A. Emanuel not only for making a new version of his convection scheme available to me, but also for leading many stimulating discussions on cumulus convection while I was at MIT. I am very thankful to M.-D. Chou and W. Ridgway of NASA/GSFC for providing me with their radiation code. Discussions with Prof. Yuk L. Yung were very helpful to my understanding of non-equilibrium thermodynamics, while discussions with Professor J. David Neelin were very helpful to my understanding of dynamical systems. Thanks are also due to Maria Carmen M. Lemos and Margaret S. Rae for reading the manuscript. Moreover, I would like to thank three anonymous reviewers for their suggestions and helpful criticisms that substantially improved the original paper. Finally, I would like to thank Caltech's Planetary Science Division, the LLNL RAS Division, and the University of Arizona's Atmospheric Sciences Department for supporting this study.

REFERENCES

Arakawa, A. 1969. Parameterization of cumulus convection. In: *Proceedings of the WMO/IUGG Symposium of Numerical weather prediction*, pp. 1–6. Japan Meteorological Society, Tokyo.

Asselin, R. 1972. Frequency filter for time integrations. *Mon. Wea. Rev.* **100**, 437–490.

Betts, A. K. 1982. Saturation point analysis of moist convective overturning. *J. Atmos. Sci.* **39**, 1484–1505.

Betts, A. K. 1985. Mixing line analysis of clouds and cloudy boundary layers. *J. Atmos. Sci.* **42**, 2751–2763.

Betts, A. K. and Ridgway, W. 1988. Coupling of the radiative, convective, and surface fluxes over the equatorial Pacific. *J. Atmos. Sci.* **45**, 522–536.

Brunt, D. 1941. *Physical and dynamical meteorology*. Cambridge University Press, Cambridge, 428 pp.

Chou, M.-D., Krats, D. P. and Ridgway, W. 1991. Infrared radiation parameterization in numerical climate models. *J. Climate* **4**, 424–437.

Chou, M.-D. 1992. A solar radiation model for use in climate studies. *J. Atmos. Sci.* **49**, 762–772.

Emanuel, K. A. 1991. A scheme for representing cumulus convection in large-scale models. *J. Atmos. Sci.* **48**, 2313–2335.

Emanuel, K. A., Neelin, J. D. and Bretherton, C. S. 1994. On large-scale circulations in convecting atmospheres. *Q. J. R. Meteorol. Soc.* **120**, 1111–1143.

Glansdorff, P. and Prigogine, I. 1971. *Thermodynamic theory of structure, stability and fluctuations.* Wiley Interscience, 306 pp.

Hansen, J., Russell, G., Rind, D., Stone, P., Lacis, A., Lebedeff, S., Ruedy, R. and Travis, L. 1983. Efficient 3-dimensional global models for climate studies. Models I and II. *Mon. Weather Rev.* **111**, 609–662.

Hilbert, D. 1912. Begründung der elementaren Strahlungstheorie. *Physik Zeitschrift* **13**, 1056–1064.

Hunt, K. L. C. and Hunt, P. M. 1987. Dissipation in steady states of chemical systems and deviations from minimum entropy production. *Physica* **147A**, 48–60.

Ingersoll, A. P. 1969. The runaway greenhouse. A history of water on Venus. *J. Atmos. Sci.* **26**, 1191–1198.

Kasting, J. F., Pollack, J. B. and Crisp, D. 1984. Effects of high CO_2 levels on surface temperature and atmospheric oxidation state on the early Earth. *J. Atmos. Chem.* **1**, 423–428.

Kelvin, W. T. 1862. On the convective equilibrium of temperature in the atmosphere. *Mem. Phil. Soc. Manchester* **2**, 125.

Komabayasi, M. 1967. Discrete equilibrium temperatures of a hypothetical planet with the atmosphere and the hydrosphere of one component-two phase system under constant solar radiation. *J. Meteor. Soc. Japan* **45**, 137–138.

Lindzen, R. S., Hou, A. Y. and Farrel, B. F. 1982. The role of convective model choice in calculating the climate impact of doubling CO_2. *J. Atmos. Sci.* **39**, 1189–1205.

Manabe, S. and Strickler, R. F. 1964. Thermal equilibrium of the atmosphere with a convective adjustment. *J. Atmos. Sci.* **21**, 361–385.

Manabe, S. and Wetherald, R. T. 1967. Thermal equilibrium of the atmosphere with a given distribution of relative humidity. *J. Atmos. Sci.* **24**, 241–259.

Manabe, S., Smagorinsky, J. and Strickler, Robert F. 1965. Simulated climatology of a general circulation model with a hydrologic cycle. *Mon. Wea. Rev.* **93**, 769–798.

McClatchey, R. A., Fenn, R. W., Selby, J. E. A., Volz, F. E. and Garing, J. S., 1972. *Optical properties of the atmosphere.* Air Force Cambridge Research Laboratories, Environmental Research Papers, No. 411.

Mobbs, S. D. 1982. Extremal principles for global climate models. *Quart. J. R. Met. Soc.* **108**, 535–550.

Nakajima, S., Hayashi Y.-Y. and Abe, Y. 1992. A study on the "Runaway Greenhouse Effect" with a one-dimensional radiative-convective equilibrium model. *J. Atmos. Sci.* **49**, 2256–2266.

Paltridge, G. W. 1981. Thermodynamic dissipation and the global climate system. *Quart. J. R. Met. Soc.* **107**, 531–547.

Pelkowski, J. 1993. Approximating the source function of an atmosphere in radiative equilibrium. A variational method. *Beitr. Atmosph.* **66**, 259–271.

Pollack, J. B. 1971. A nongray calculation of the runaway greenhouse. Implications for Venus's past and present. *Icarus* **14**, 295–306.

Prigogine, I. 1947. *Etude thermodynamique des processes irreversible*, Desoer, Liege.

Ramanathan, V. 1981. The role of ocean-atmosphere interactions in the CO_2 climate problem. *J. Atmos. Sci.* **38**, 918–930.

Ramanathan, V. and Collins, W. 1991. Thermodynamic regulation of ocean warming by cirrus clouds deduced from observations of the 1987 El Niño. *Nature* **351**, 27–32.

Raval, A. and Ramanathan, V. 1989. Observational determination of the greenhouse effect. *Nature* **342**, 758–761.

Rennó, N. O. 1992. *Cumulus convection parameterization and numerical modelling of moist atmospheres.* PhD thesis. Mass. Inst. of Technol., Cambridge, MA, 297 pp.

Rennó, N. O. 1994. Multiple equilibria in radiative-convective atmospheres. In: *Proceedings of the AGU Fall Meeting*, p. 129. American Geophysical Union, Washington.

Rennó, N. O., Emanuel, K. A. and Stone, P. H. 1994a. A radiative-convective model with an explicit hydrological cycle (1). Formulation and sensitivity to model parameters. *J. Geophys. Res.* **99**(D7), 14,429–14,441.

Rennó, N. O., Stone, P. H. and Emanuel, K. A. 1994b. A radiative-convective model with an explicit hydrological cycle 2. Sensitivity to large changes in solar forcing. *J. Geophys. Res.* **99**(D8), 17001–17020.

Rennó, N. O. and Williams, E. R. 1995. Quasi-Lagrangian measurements in convective boundary layer plumes and their implications for the calculation of CAPE. *Mon. Wea. Rev.* **123**, 2733–2742.

Rennó, N. O. and Ingersoll, A. P. 1996. Natural convection as a heat engine. A theory for CAPE. *J. Atmos. Sci.* **53**, 572–585.

Sarachik, E. S. 1978. Tropical sea surface temperature: An interactive one-dimensional atmosphere ocean model. *Dyn. Atmos. Oceans* **2**, 455–469.

Simpson, G. C. 1927. Some studies in terrestrial radiation. *Mem. R. Meteorol. Soc.* **2**, No. 16.

Somerville, R. C. J., Stone, P. H., Harlen, M., Hansen, J. E., Hogan, J. S., Druyan, L. M., Russell, G., Lacis, A. A., Quirk, W. J. and Tenenbaum, J. 1974. The GISS model of the global atmosphere. *J. Atmos. Sci.* **31**, 84–117.

Wang, W.-C. and Stone, P. H. 1980. Effect of ice-albedo feedback on global sensitivity in a one-dimensional radiative-convective Climate Model. *J. Atmos. Sci.* **37**, 545–552.